

# Finding the Most Transferable Tasks for Brain Image Segmentation

Yicong Li, Yang Tan, Jingyun Yang, Yang Li, Xiao-Ping Zhang  
Tsinghua-Berkeley Shenzhen Institute  
Tsinghua University  
Shenzhen, China  
yangli@sz.tsinghua.edu.cn

**Abstract**—Although many studies have successfully applied transfer learning to medical image segmentation, very few of them have investigated the selection strategy when multiple source tasks are available for transfer. In this paper, we propose a prior knowledge guided and transferability based framework to select the best source tasks among a collection of brain image segmentation tasks, to improve the transfer learning performance on the given target task. The framework consists of modality analysis, RoI (region of interest) analysis, and transferability estimation, such that the source task selection can be refined step by step. Specifically, we adapt the state-of-the-art analytical transferability estimation metrics to medical image segmentation tasks and further show that their performance can be significantly boosted by filtering candidate source tasks based on modality and RoI characteristics. Our experiments on brain matter, brain tumor, and white matter hyperintensities segmentation datasets reveal that transferring from different tasks under the same modality is often more successful than transferring from the same task under different modalities. Furthermore, within the same modality, transferring from the source task that has stronger RoI shape similarity with the target task can significantly improve the final transfer performance. And such similarity can be captured using the Structural Similarity index in the label space.

**Index Terms**—transfer learning, medical image analysis, source selection

## I. INTRODUCTION

Supervised deep learning algorithm requires an abundant amount of annotated data to obtain a well-trained model that can make accurate predictions. Such a requirement severely limits the application of deep learning in the medical domain since acquiring and labeling medical data can be very expensive and time-consuming. A commonly used solution is transfer learning [1]: pre-training a model on a source task where sufficient annotated data exists and fine-tuning the model on the desired target task where only a small amount of annotated data is available. A key question to the success of transfer learning between source and target tasks is what source task shall we transfer from given a target task (i.e., what to transfer). That is, if we transfer knowledge from a less related source task, it may inversely hurt the performance on the target task, a phenomenon known as negative transfer [2]. Although many studies have already successfully applied transfer learning to medical image analysis problems [3]–[5], very few of them have investigated how to select the best

source tasks. Hence in this work, we aim to systematically tackle the *source selection problem*, focusing particularly on the most dominant image segmentation tasks.

An effective source selection strategy requires a good understanding of what factors affect the transfer performance for medical segmentation tasks. Several experimental studies have investigated the transfer learning performance in medical image analysis. In [6], advantages and disadvantages of several transfer learning strategies for medical image segmentation tasks are explored, such as which component of a CNN model is better to transfer. Weatheritt et al. [7] analyze the impacts of different choices of data pre-processing methods, tasks, and amount of data used on the final transfer performance. Unfortunately, these studies haven't fully investigated how detailed characteristics of source tasks can influence transfer learning performance. Particularly, for medical image segmentation, image characteristics of source tasks such as the modality and the geometric shape of the segmentation region of interest (RoI) vary greatly due to the fundamental differences in scanner protocols, imaging procedures, lesion positions, etc. Such variations will definitely affect the final transfer learning performance on the target task.

To tackle the source selection problem systematically, we need a quantitative way to rank the transfer performance of source tasks. Recent studies have proposed different methods to estimate the *knowledge transferability* between source and target tasks for natural images. Transferability reveals how easy it is to transfer knowledge learned from a source task to a target task. Bao et al. [8] takes an information theoretic approach and develops a computable metric called H-score to estimate the knowledge transferability between datasets for image classification problems. Under the assumption that the inputs of source and target tasks share the same domain, Tran et al. [9] uses NCE, negative conditional entropy, to evaluate transferability. In [10], a new metric called LEEP is proposed. It makes predictions based on the expected empirical conditional distribution between source and target labels. More recently, Tan et al. [11] proposes an optimal transport based conditional entropy (OTCE) metric to analytically predict transfer performance for supervised classification problems, which has been further extended to evaluate segmentation problems as well [12]. However, these works focus on finding a general-purpose transferability metric purely based on fea-

This research is funded by Natural Science Foundation of China 62001266. Supplementary materials are available in this arXiv version.

ture effectiveness without consideration of prior knowledge (e.g., image characteristics) about tasks, such as modality difference and RoI shape similarity between source and target tasks in the medical image domain.

As such, in this work, we propose a novel source selection framework that leverages the prior knowledge of medical image segmentation tasks for reducing the computation time and improving the selection accuracy of existing transferability metrics, so as to create a systematic way to select the best source tasks for a given target task. We choose brain image segmentation datasets for our experiments since it is one of the most challenging and time-consuming clinical procedures for diagnosing brain disorders, whose demand has been increasing in recent years. In summary, our main contributions are:

- **A prior knowledge guided and transferability based source selection framework.** The framework incorporates prior knowledge of medical image segmentation tasks with transferability estimation metrics to select the best source tasks for transfer learning given a target task.
- **An analysis of the relationship between image characteristics and transfer learning performance.** We extensively conduct transfer learning experiments under the cross-modality or cross-task setting and conclude that transferring from a different task under the same modality is often more beneficial than transferring from the same task under a different modality. We also quantitatively show that within the same modality, transferring from the source task that has stronger RoI shape similarity with the target task outperforms transferring from those less similar ones.

## II. METHODS

### A. Problem Description

In a typical source selection problem, we are given  $K$  pre-trained source models  $\{\theta_s\}_{k=1}^K$  corresponding to  $K$  source task  $\{T_s\}_{k=1}^K$  and a target task  $T_t$ . The problem goal is to find out which source task  $T_s$  we should transfer from in order to achieve the best transfer performance on the target task  $T_t$ .

The most common source selection approach is to fine-tune each source model on the target task to obtain a transfer accuracy on the target test set. This transfer accuracy is called the *ground truth transferability*, which can be represented by a certain segmentation accuracy evaluation metric, such as Dice score. Then the task that corresponds to the source model that achieves the best transfer accuracy will be selected as the most appropriate source. However, this naive method is very computationally expensive and may become very inefficient when  $K$  is large. Therefore, analytical methods are developed to estimate the transferability without fine-tuning each source model on the target task to save time and resources. The ranking of transferability scores between source and target tasks produced by such analytical methods should well correlate with the ranking given by the ground truth transferability scores so that top-performing sources can be selected accurately but in a less time-consuming way.

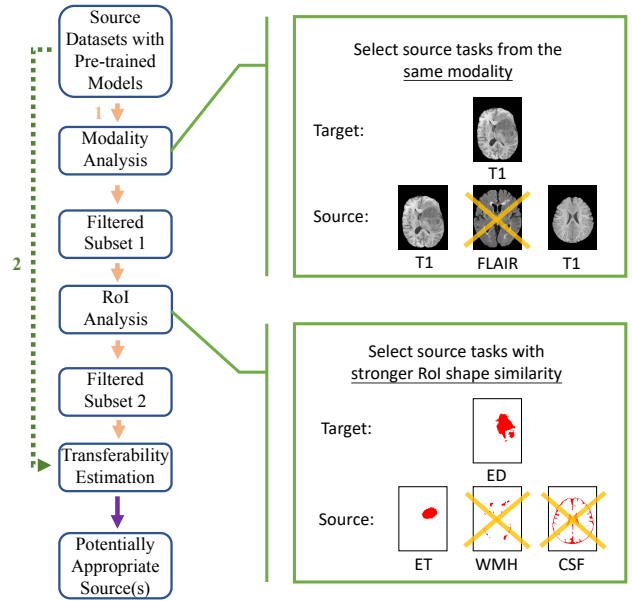


Fig. 1. Prior knowledge guided and transferability based source selection framework. Path 1: do modality analysis and RoI analysis, then use transferability estimation metrics. Path 2: apply transferability estimation metrics directly on the source tasks. T1: t1-weighted modality, FLAIR: fluid-attenuated inversion recovery modality, ED: edematous tissue, ET: enhancing tumor, WMH: white matter hyperintensities, CSF: cerebrospinal fluid.

### B. Prior Knowledge Guided and Transferability Based Source Selection Framework

Unfortunately, analytical transferability estimation metrics like H-score and OTCE are designed for natural images, thus their performance in the medical image domain is not guaranteed. Inspired by the differences in modalities and RoI shapes of medical image segmentation tasks, we propose a source selection framework that incorporates the analysis of image characteristics with current state-of-the-art transferability estimation metrics, as shown in Fig. 1.

Given a pool of source tasks and a target task, we propose to analyze the image characteristics of tasks before computing transferability estimation metrics (Path 1 in Fig. 1). Specifically, our framework consists of three steps:

1) **Modality Analysis:** Select source tasks that are under the same modality as the target task to generate Subset 1 (we define a subset as a smaller group of tasks selected from a bigger group of tasks).

2) **RoI Analysis:** Within Subset 1 (in which source tasks are under the same modality as the target task), select source tasks whose RoI shapes are more similar to that of the target task by calculating the shape similarity to generate Subset 2. Specifically, we propose to use structural similarity index measure (SSIM) [13] to quantify the RoI shape similarity. In our transfer learning context, given a source task  $T_s$  with its label set  $Y_s$  and a target task  $T_t$  with its label set  $Y_t$ , we compute their RoI shape similarity as:

$$\text{RoI-Sim}(T_s, T_t) = \text{SSIM}(Y_s, Y_t). \quad (1)$$

More details on SSIM can be found in the supplementary materials.

3) **Transferability Estimation:** Within Subset 2, we apply a certain analytical transferability estimation metric to select potentially appropriate source tasks. In this work, we choose H-score [8] or OTCE [12] as the metric.

In the task transfer learning setting, let  $(X_s, Y_s)$  and  $(X_t, Y_t)$  represent the input and output random variables of the source and target tasks, respectively. Given a source model  $\theta_s$  pre-trained on a source task, we denote the feature of source and target data  $X_s, X_t$  extracted by the source model  $\theta_s$  as  $\theta_s(X_s)$  and  $\theta_s(X_t)$ . Assuming the same input domain  $P(\theta_s(X_s)) = P(\theta_s(X_t))$ , H-score measures the transferability of  $\theta_s$  with respect to the target task as

$$\mathcal{H}(\theta_s, X_t, Y_t) = \text{tr}(\text{cov}(\theta_s(X_t))^{-1} \text{cov}(\mathbb{E}_{P_{X_t|Y_t}}[\theta_s(X_t)|Y_t])), \quad (2)$$

where the covariance (*cov*) and the expectation are estimated empirically from data [8]. H-score is originally designed to handle classification tasks, therefore we adapt it to segmentation tasks by considering each pixel in the image as an individual classification task and calculating an H-score for each of them. Then the final H-score is the arithmetic mean of all pixel-wise scores:

$$H\text{-score}(T_s, T_t) = \frac{1}{N} \sum_{j=1}^N \mathcal{H}(\theta_s^j, X_t, Y_t^j), \quad (3)$$

where  $N$  is the total number of pixels in the segmentation label image,  $\theta_s^j$  represents the source model feature mapping corresponding to the  $j$ th pixel, and  $Y_t^j$  represents the segmentation label of the  $j$ th pixel. We choose H-score because it is highly efficient and effective when the segmentation tasks have similar input distributions but different RoIs.

The OTCE score is a versatile transferability metric for both the cross-domain and the cross-task transfer scenarios. To compute OTCE, we first use the pre-trained source model  $\theta_s$  to produce the pixel-wise feature sets  $D_s = \{(v_s^i, y_s^i)\}_{i=1}^{N_s}$  and  $D_t = \{(v_t^i, y_t^i)\}_{i=1}^{N_t}$  for the source and target tasks respectively, where  $v_d^i, y_d^i$ , and  $N_d$  denotes the pixel-wise feature vector, pixel-wise label, and the total number of pixels in all images of task  $d \in \{s, t\}$ , respectively. Next, we find the optimal coupling matrix of size  $N_s \times N_t$  between source and target features by solving the following regularized Optimal Transport (OT) problem:

$$OT(D_s, D_t) \triangleq \min_{\pi \in \Pi(D_s, D_t)} \sum_{i,j=1}^{N_s, N_t} \|v_s^i - v_t^j\|_2^2 \pi_{ij} + \epsilon H(\pi), \quad (4)$$

where  $H(\pi) = -\sum_{i=1}^{N_s} \sum_{j=1}^{N_t} \pi_{ij} \log \pi_{ij}$  is the entropic regularizer with  $\epsilon = 0.1$ . Since the optimal coupling matrix  $\pi^*$  represents the empirical joint probability distribution of source and target pixel-wise features, under mild assumptions, the empirical joint probability distribution of source and target labels can be written as

$$\hat{P}(y_s, y_t) = \sum_{i,j: y_s^i = y_s, y_t^j = y_t} \pi_{ij}^*. \quad (5)$$

Finally, the OTCE score can be computed as the negative conditional entropy between the source and target labels:

$$\begin{aligned} OTCE(T_s, T_t) &= -H(Y_t|Y_s) \\ &= \sum_{y_t \in \mathcal{Y}_t} \sum_{y_s \in \mathcal{Y}_s} \hat{P}(y_s, y_t) \log \frac{\hat{P}(y_s, y_t)}{\sum_{y_t \in \mathcal{Y}_t} \hat{P}(y_s, y_t)}, \end{aligned} \quad (6)$$

where  $\mathcal{Y}_s$  and  $\mathcal{Y}_t$  denote the source and target pixel-wise label space. More details of OTCE for semantic segmentation can be found in [12].

As an ablation study of our source selection framework, a baseline approach (Path 2 in Fig. 1) is directly computing the transferability estimation metric on all source tasks without considering the image characteristics of tasks.

### III. EXPERIMENTAL SETTINGS AND RESULTS

#### A. Datasets

We perform experiments on three publicly available brain MRI segmentation datasets: FeTS 2021 [14]–[16] for brain tumor segmentation, iSeg-2019 [17] for brain matter segmentation, and WMH [18] for white matter hyperintensities segmentation.

For each sample in FeTS 2021 dataset, volumes of 4 modalities are available, including T1-weighted (T1), T2-weighted (T2), Fluid-Attenuated Inversion Recovery (FLAIR), and T1-Weighted Contrast-Enhanced (T1CE). The volume size is  $240 \times 240 \times 155$ . Corresponding labels of edematous tissue (ED), enhancing tumor (ET), and necrotic tumor core (NCR) are manually segmented by clinical experts. For each sample in iSeg-2019 dataset, volumes of 2 modalities are available, including T1 and T2. The volume size is  $144 \times 192 \times 256$ . Corresponding labels of white matter (WM), gray matter (GM), and cerebrospinal fluid (CSF) are manually segmented by clinicians. The WMH dataset consists of 60 brain MRI volumes of FLAIR modality with manual annotations of white matter hyperintensities from three different institutes, namely, VU Amsterdam (A), NUHS Singapore (S), and UMC Utrecht (U). Volume sizes are  $132 \times 256 \times 83$ ,  $256 \times 232 \times 48$ , and  $240 \times 240 \times 48$  for the three institutes, respectively. Corresponding labels of white matter hyperintensities (WMH) are manually segmented by clinical experts.

To provide enough tasks for experimental analysis, we reorganize these three datasets into a collection of binary segmentation tasks on every available modality. Examples of images from these three datasets with their corresponding labels are visualized in Fig. 2.

#### B. Model Architecture and Transfer Learning Strategy

Since the goal of this work is to investigate the source selection problem rather than trying to achieve state-of-the-art performance on medical image segmentation tasks, we use the same model architecture for all experiments presented in this paper, a classic 2D U-Net [19]. As for the transfer learning strategy, we follow the most common way which is pre-training the model on a source task and fine-tuning it on a target task. During the fine-tuning stage, the encoder is frozen

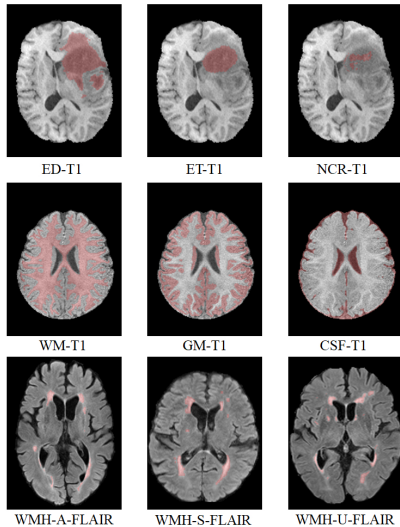


Fig. 2. Examples of images from FeTS 2021, iSeg-2019, and WMH datasets with their corresponding labels. In FeTS 2021 dataset, e.g., “ED-T1” denotes edematous tissue segmentation on T1 modality. In iSeg-2019 dataset, e.g., “WM-T1” denotes white matter segmentation on T1 modality. In WMH dataset, e.g., “WMH-A-FLAIR” denotes white matter hyperintensities segmentation on FLAIR modality from institute A.

TABLE I  
COMPARISONS OF CROSS-TASK TRANSFER AND CROSS-MODALITY TRANSFER ON FETS 2021 (TOP) AND ISEG-2019 (BOTTOM) DATASETS.

Target	Source <sup>a</sup>	Average Dice <sup>b</sup>
ET-T1CE	ET-T1, ET-T2, ET-FLAIR ED-T1CE, NCR-T1CE	0.755 <b>0.821</b>
ED-T1CE	ED-T1, ED-T2, ED-FLAIR ET-T1CE, NCR-T1CE	0.731 <b>0.786</b>
NCR-T1CE	NCR-T1, NCR-T2, NCR-FLAIR ET-T1CE, ED-T1CE	0.726 <b>0.782</b>
WM-T1	WM-T2 GM-T1, CSF-T1	0.864 <b>0.877</b>
GM-T1	GM-T2 WM-T1, CSF-T1	0.881 <b>0.892</b>
CSF-T1	CSF-T2 WM-T1, GM-T1	<b>0.935</b> 0.934

<sup>a</sup>Green/Blue: cross-modality/task transfer.

<sup>b</sup>Red: better transfer performance.

and only the parameters of the decoder are updated. See the supplementary materials for details on the model architecture and the training process.

### C. Verification of Modality Analysis

In Modality Analysis, we select source tasks having the same modality as the target task as the candidate sources (Subset 1). To verify the correctness of this design, we conduct experiments using source and target tasks from the multi-modal datasets FeTS 2021 and iSeg-2019.

As shown in Table I, transferring from different tasks under the same modality (sources in blue) outperforms transferring from the same task under different modality (sources in green) in almost all trials (5 out of 6, the scores of the only exception are very close) with a significant margin (average Dice scores in red). Such a finding suggests that for the common transfer

learning strategy of pre-training and fine-tuning, matching different source and target data modalities is harder than re-learning a new task within the same modality.

### D. Verification of RoI Analysis

In RoI Analysis, within Subset 1, we select source tasks whose RoI shapes are more similar to that of the target task by calculating the shape similarity using SSIM, and then generate Subset 2. To verify this choice, we conduct experiments using source and target tasks from all three datasets. Specifically, our experiment includes both the setting when the source and target tasks are from the same dataset (same-dataset), and when they are from different datasets (cross-dataset) to show the effectiveness and generalizability of our framework.

As shown in Table II and III, we first compute the RoI shape similarity score (RoI-Sim) between the source and the target task of the same modality. Then, we also perform transfer learning experiments to obtain the ground truth transfer accuracy between them. According to the results, we can conclude that in both same-dataset (Table II) and cross-dataset (Table III) settings, when the RoI shape similarity between the source and the target task is stronger (the RoI-Sim score in red), the transfer performance is often (16 out of 18 trials) better (the Dice score in red). Such a finding suggests that within the same modality, SSIM can serve as an indicator to rank the performances of transfer learning from different source tasks to the target task.

### E. Results of Source Selection

For the source selection experiments, we use FeTS 2021 dataset. This dataset is further split into 22 partitions by the provider, according to different institutions and information extracted from images. Thus, each partition can be seen as an individual domain. Here, we additionally denote a task by “Task-Partition-Modality”, e.g., “ET-14-T1” represents the task of enhancing tumor segmentation on T1 modality using data from partition 14. In total, 16 source tasks (ED/NCR-13/14/17/18-T1/T2) and 2 target tasks (ET-22-T2 and ET-20-T1) are used to conduct two groups of source selection experiments. The ground truth transfer learning results and the calculated transferability results on two target tasks are shown in Table IV and Table V.

The result of source selection is a ranking of source tasks according to their transfer performance on a given target task. The **ground truth ranking** is obtained by sorting the Dice scores after fine-tuning each source task on a given target task. A higher Dice score indicates better transferability. The **baseline ranking prediction** is obtained by directly computing and sorting H-scores or OTCE scores on all source tasks (Path 2 in Fig. 1). A higher H-score or OTCE score indicates better transferability. The **ranking prediction proposed by our framework** is obtained through combining prior knowledge with transferability estimation metrics, as indicated by Path 1 in Fig. 1. We take Table IV as an example to illustrate how to obtain the ranking prediction with our proposed framework. Given a target task of ET-22-T2, we notice that this task is

TABLE II

ANALYSIS OF RELATIONSHIP BETWEEN ROI SHAPE SIMILARITY AND TRANSFER PERFORMANCE ON FETS 2021 (TOP) AND ISEG-2019 (BOTTOM) DATASETS.

Target	Source	Dice <sup>a</sup>	RoI-Sim <sup>b</sup>	Target	Source	Dice <sup>a</sup>	RoI-Sim <sup>b</sup>	Target	Source	Dice <sup>a</sup>	RoI-Sim <sup>b</sup>
ED-T1	ET-T1	<b>0.757</b>	<b>0.987</b>	ED-T2	ET-T2	<b>0.811</b>	<b>0.987</b>	ED-FLAIR	ET-FLAIR	<b>0.773</b>	<b>0.987</b>
	NCR-T1	0.738	0.984		NCR-T2	0.802	0.984		NCR-FLAIR	0.760	0.984
ET-T1	ED-T1	<b>0.693</b>	<b>0.987</b>	ET-T2	ED-T2	<b>0.703</b>	<b>0.987</b>	ET-FLAIR	ED-FLAIR	<b>0.681</b>	<b>0.987</b>
	NCR-T1	0.672	0.985		NCR-T2	0.660	0.985		NCR-FLAIR	0.613	0.985
NCR-T1	ED-T1	0.585	0.984	NCR-T2	ED-T2	<b>0.598</b>	0.984	NCR-FLAIR	ED-FLAIR	<b>0.558</b>	0.984
	ET-T1	<b>0.602</b>	<b>0.985</b>		ET-T2	0.578	<b>0.985</b>		ET-FLAIR	0.550	<b>0.985</b>
WM-T1	GM-T1	<b>0.885</b>	<b>0.844</b>	WM-T2	GM-T2	<b>0.852</b>	<b>0.844</b>	-	-	-	-
	CSF-T1	0.868	0.824		CSF-T2	0.815	0.824	-	-	-	-
GM-T1	WM-T1	<b>0.893</b>	<b>0.844</b>	GM-T2	WM-T2	<b>0.879</b>	<b>0.844</b>	-	-	-	-
	CSF-T1	0.891	0.838		CSF-T2	0.863	0.838	-	-	-	-
CSF-T1	WM-T1	0.925	0.824	CSF-T2	WM-T2	0.909	0.824	-	-	-	-
	GM-T1	<b>0.942</b>	<b>0.838</b>		GM-T2	<b>0.916</b>	<b>0.838</b>	-	-	-	-

<sup>a</sup>Red: better transfer performance. <sup>b</sup>Red: stronger RoI shape similarity.

TABLE III

ANALYSIS OF RELATIONSHIP BETWEEN ROI SHAPE SIMILARITY AND TRANSFER PERFORMANCE ACROSS FETS 2021 AND WMH DATASETS.

Target	Source	Dice <sup>a</sup>	RoI-Sim <sup>b</sup>
WMH-U-FLAIR	NCR-FLAIR	<b>0.650</b>	<b>0.979</b>
	ET-FLAIR	0.644	0.978
	ED-FLAIR	0.578	0.967
WMH-S-FLAIR	NCR-FLAIR	<b>0.542</b>	<b>0.982</b>
	ET-FLAIR	<b>0.542</b>	0.981
	ED-FLAIR	0.531	0.970
WMH-A-FLAIR	NCR-FLAIR	<b>0.572</b>	<b>0.985</b>
	ET-FLAIR	0.538	0.984
	ED-FLAIR	0.547	0.973

<sup>a</sup>Red: better transfer performance.<sup>b</sup>Red: stronger RoI shape similarity.

TABLE IV

TRANSFER LEARNING AND TRANSFERABILITY ESTIMATION RESULTS ON THE TARGET TASK OF ET-22-T2.

Target	Source <sup>a</sup>	Dice	H-score	OTCE
ET-22-T2	ED-14-T1	0.664	-0.0380	-0.0395
	<b>ED-14-T2</b>	0.703	0.1887	-0.0226
	NCR-14-T1	0.646	0.8990	-0.0395
	NCR-14-T2	0.660	0.5140	-0.0383
	ED-13-T1	0.657	0.4142	-0.0407
	<b>ED-13-T2</b>	0.695	1.4031	-0.0356
	NCR-13-T1	0.628	5.0050	-0.0407
	NCR-13-T2	0.683	10.5247	-0.0401
	ED-17-T1	0.697	0.3525	-0.0435
	<b>ED-17-T2</b>	0.708	1.3327	-0.0389
	NCR-17-T1	0.612	1.5211	-0.0436
	NCR-17-T2	0.681	6.6535	-0.0433
	ED-18-T1	0.675	0.1070	-0.0435
	<b>ED-18-T2</b>	0.707	0.2776	-0.0273
	NCR-18-T1	0.664	0.9038	-0.0436
	NCR-18-T2	0.666	2.2038	-0.0394

<sup>a</sup>Underlined sources: Subset 1. Sources in red: Subset 2.

under the T2 modality. According to our modality analysis in Section II-B1, we should select those 8 source tasks under the same modality as the target task (underlined in Table IV). This procedure forms Subset 1. Next, according to our RoI analysis in Section II-B2, within the T2 modality, the

TABLE V

TRANSFER LEARNING AND TRANSFERABILITY ESTIMATION RESULTS ON THE TARGET TASK OF ET-20-T1.

Target	Source <sup>a</sup>	Dice	H-score	OTCE
ET-20-T1	<b>ED-14-T1</b>	0.636	1.5433	-0.0320
	ED-14-T2	0.609	0.2268	-0.0330
	<u>NCR-14-T1</u>	0.560	3.2383	-0.0325
	NCR-14-T2	0.627	2.5139	-0.0330
	<b>ED-13-T1</b>	0.593	1.7564	-0.0333
	ED-13-T2	0.636	1.3293	-0.0347
	<u>NCR-13-T1</u>	0.498	2.4574	-0.0342
	NCR-13-T2	0.610	6.5037	-0.0346
	<b>ED-17-T1</b>	0.680	2.5901	-0.0351
	ED-17-T2	0.571	-3.2459	-0.0363
	<u>NCR-17-T1</u>	0.581	25.7285	-0.0361
	NCR-17-T2	0.532	40.6843	-0.0363
	<b>ED-18-T1</b>	0.613	0.0901	-0.0357
	ED-18-T2	0.616	0.3164	-0.0355
	<u>NCR-18-T1</u>	0.632	0.2743	-0.0361
	NCR-18-T2	0.637	1.6508	-0.0362

<sup>a</sup>Underlined sources: Subset 1. Sources in red: Subset 2.

RoI shape similarity between ED and ET estimated by SSIM is higher than that between ED and NCR, thus we should select those 4 source tasks (colored in red in Table IV) of ED segmentation rather than NCR segmentation. This procedure forms Subset 2. Finally, we apply the analytical transferability estimation metric on source tasks in Subset 2 and obtain their predicted ranking. As for Table V, the source selection procedure using our proposed framework is similar.

The performance of source selection methods is often evaluated by comparing the difference between the ground truth transfer performance ranking and the predicted transfer performance ranking. Here, we use Spearman's footrule [20] to quantify the difference between the two rankings. More details on Spearman's footrule can be found in the supplementary materials. The performance evaluation on selecting the top 1-4 source tasks is shown in Table VI. For both target tasks and under all top 1-4 source selection settings, when following our proposed prior knowledge guided and transferability based framework, the difference between the

TABLE VI  
EVALUATION OF SOURCE SELECTION PERFORMANCE WITH/WITHOUT  
PRIOR KNOWLEDGE.

Target	Method <sup>a</sup>	Top 1 <sup>b</sup>	Top 2 <sup>b</sup>	Top 3 <sup>b</sup>	Top 4 <sup>b</sup>
ET-22-T2	H-score w/o PK	5	10	22	27
	H-score w/ PK	4	5	6	7
	OTCE w/o PK	2	2	4	12
	OTCE w/ PK	2	2	4	7
ET-20-T1	H-score w/o PK	14	24	30	40
	H-score w/ PK	0	9	9	13
	OTCE w/o PK	2	14	17	23
	OTCE w/ PK	2	11	13	17

<sup>a</sup>PK: prior knowledge.

<sup>b</sup>Top 1-4: required number of selected sources. Red: better performance.

predicted ranking and the ground truth ranking is reduced. This suggests that prior knowledge about the medical image segmentation tasks, including modality and RoI characteristics, can indeed improve the current state-of-the-art transferability metrics' ability to successfully select source tasks with better transfer performance. Besides, these results also reveal that current transferability estimation metrics are not sufficient to handle the large gaps between source and target tasks and thus require further refinement, particularly in the medical domain.

#### IV. CONCLUSION

We propose a prior knowledge guided and transferability based framework to tackle the source selection problem in transfer learning for brain image segmentation tasks. We are the first to apply state-of-the-art transferability estimation metrics to the medical image segmentation domain. Different from the common procedure that directly applies these metrics, our framework further considers the prior knowledge of the given source and target tasks when selecting sources. Specifically, we perform modality analysis and RoI analysis to select a subset of source tasks and then only compute the metric within this subset. Modality analysis shows that transferring from different tasks under the same modality is better than transferring from the same task under different modalities. RoI Analysis shows that stronger RoI shape similarity between the source and the target task often leads to better transfer performance. Consequently, by incorporating image characteristics of modality difference and RoI similarity into the framework, source selection experiments suggest that the performance of transferability estimation metrics like H-score and OTCE on the source selection problem can be significantly enhanced. We envision that this framework can be used on other medical image datasets besides brain images.

#### REFERENCES

- [1] Sinno Jialin Pan and Qiang Yang, "A survey on transfer learning," *IEEE Transactions on knowledge and data engineering*, vol. 22, no. 10, pp. 1345–1359, 2009.
- [2] Zirui Wang, Zihang Dai, Barnabás Póczos, and Jaime Carbonell, "Characterizing and avoiding negative transfer," in *Proceedings of the IEEE/CVF Conference on Computer Vision and Pattern Recognition*, 2019, pp. 11293–11302.
- [3] Haibo Huang, Haobo Chen, Haohao Xu, Ying Chen, Qihui Yu, Yehua Cai, and Qi Zhang, "Cross-tissue/organ transfer learning for the segmentation of ultrasound images using deep residual u-net," *Journal of Medical and Biological Engineering*, vol. 41, no. 2, pp. 137–145, 2021.
- [4] Daniel S Kermany, Michael Goldbaum, Wenjia Cai, Carolina CS Valentin, Huiying Liang, Sally L Baxter, Alex McKeown, Ge Yang, Xiaokang Wu, Fangbing Yan, et al., "Identifying medical diagnoses and treatable diseases by image-based deep learning," *Cell*, vol. 172, no. 5, pp. 1122–1131, 2018.
- [5] Sihong Chen, Kai Ma, and Yefeng Zheng, "Med3d: Transfer learning for 3d medical image analysis," *arXiv preprint arXiv:1904.00625*, 2019.
- [6] Yang Wen, Leitong Chen, Chuan Zhou, Yu Deng, Huiru Zeng, Shuo Xi, and Rui Guo, "On the effective transfer learning strategy for medical image analysis in deep learning," in *2020 IEEE International Conference on Bioinformatics and Biomedicine (BIBM)*. IEEE, 2020, pp. 827–834.
- [7] Jack Weatheritt, Daniel Rueckert, and Robin Wolz, "Transfer learning for brain segmentation: Pre-task selection and data limitations," in *Annual Conference on Medical Image Understanding and Analysis*. Springer, 2020, pp. 118–130.
- [8] Yajie Bao, Yang Li, Shao-Lun Huang, Lin Zhang, Lizhong Zheng, Amir Zamir, and Leonidas Guibas, "An information-theoretic approach to transferability in task transfer learning," in *2019 IEEE International Conference on Image Processing (ICIP)*. IEEE, 2019, pp. 2309–2313.
- [9] Anh T Tran, Cuong V Nguyen, and Tal Hassner, "Transferability and hardness of supervised classification tasks," in *Proceedings of the IEEE/CVF International Conference on Computer Vision*, 2019, pp. 1395–1405.
- [10] Cuong Nguyen, Tal Hassner, Matthias Seeger, and Cedric Archambeau, "Leep: A new measure to evaluate transferability of learned representations," in *International Conference on Machine Learning*. PMLR, 2020, pp. 7294–7305.
- [11] Yang Tan, Yang Li, and Shao-Lun Huang, "Otcce: A transferability metric for cross-domain cross-task representations," in *Proceedings of the IEEE/CVF Conference on Computer Vision and Pattern Recognition*, 2021, pp. 15779–15788.
- [12] Yang Tan, Yang Li, and Shao-Lun Huang, "Transferability estimation for semantic segmentation task," *arXiv preprint arXiv:2109.15242*, 2021.
- [13] Zhou Wang, Alan C Bovik, Hamid R Sheikh, and Eero P Simoncelli, "Image quality assessment: from error visibility to structural similarity," *IEEE transactions on image processing*, vol. 13, no. 4, pp. 600–612, 2004.
- [14] Sarthak Pati, Ujjwal Baid, Maximilian Zenk, Brandon Edwards, Micah Sheller, G Anthony Reina, Patrick Foley, Alexey Gruzdev, Jason Martin, Shadi Albarqouni, et al., "The federated tumor segmentation (fets) challenge," *arXiv preprint arXiv:2105.05874*, 2021.
- [15] G Anthony Reina, Alexey Gruzdev, Patrick Foley, Olga Perepelkina, Mansi Sharma, Igor Davidyuk, Ilya Trushkin, Maksim Radionov, Aleksandr Mokrov, Dmitry Agapov, et al., "Openfl: An open-source framework for federated learning," *arXiv preprint arXiv:2105.06413*, 2021.
- [16] Spyridon Bakas, Hamed Akbari, Aristeidis Sotiras, Michel Bilello, Martin Rozycki, Justin S Kirby, John B Freymann, Keyvan Farahani, and Christos Davatzikos, "Advancing the cancer genome atlas glioma mri collections with expert segmentation labels and radiomic features," *Scientific data*, vol. 4, no. 1, pp. 1–13, 2017.
- [17] Yue Sun, Kun Gao, Zhengwang Wu, Guannan Li, Xiaopeng Zong, Zhihao Lei, Ying Wei, Jun Ma, Xiaoping Yang, Xue Feng, et al., "Multi-site infant brain segmentation algorithms: The iseg-2019 challenge," *IEEE Transactions on Medical Imaging*, vol. 40, no. 5, pp. 1363–1376, 2021.
- [18] Hugo J Kuijff, J Matthijs Biesbroek, Jeroen De Bresser, Rutger Heinen, Simon Andermatt, Mariana Bento, Matt Berseth, Mikhail Belyaev, M Jorge Cardoso, Adria Casamitjana, et al., "Standardized assessment of automatic segmentation of white matter hyperintensities and results of the wmh segmentation challenge," *IEEE transactions on medical imaging*, vol. 38, no. 11, pp. 2556–2568, 2019.
- [19] Olaf Ronneberger, Philipp Fischer, and Thomas Brox, "U-net: Convolutional networks for biomedical image segmentation," in *International Conference on Medical image computing and computer-assisted intervention*. Springer, 2015, pp. 234–241.
- [20] Persi Diaconis and Ronald L Graham, "Spearman's footrule as a measure of disarray," *Journal of the Royal Statistical Society: Series B (Methodological)*, vol. 39, no. 2, pp. 262–268, 1977.

- [21] Zhou Wang and Alan C Bovik, "Mean squared error: Love it or leave it? a new look at signal fidelity measures," *IEEE signal processing magazine*, vol. 26, no. 1, pp. 98–117, 2009.
- [22] Hamid R Sheikh, Muhammad F Sabir, and Alan C Bovik, "A statistical evaluation of recent full reference image quality assessment algorithms," *IEEE Transactions on image processing*, vol. 15, no. 11, pp. 3440–3451, 2006.
- [23] Diederik P Kingma and Jimmy Ba, "Adam: A method for stochastic optimization," *arXiv preprint arXiv:1412.6980*, 2014.
- [24] Adam Paszke, Sam Gross, Francisco Massa, Adam Lerer, James Bradbury, Gregory Chanan, Trevor Killeen, Zeming Lin, Natalia Gimelshein, Luca Antiga, et al., "Pytorch: An imperative style, high-performance deep learning library," *Advances in neural information processing systems*, vol. 32, 2019.

## V. SUPPLEMENTARY MATERIALS

### A. Structural Similarity Index Measure (SSIM)

SSIM is often used to evaluate the visual similarity between two images. The idea is that natural images often contain highly structural information, i.e., neighboring pixels in natural images have a strong correlation. And such correlation encompasses the structural information of the object in a given environment. The human visual system is very used to extract such structural information from natural images. Therefore, the measurement of similarity given by SSIM is more in line with the perception of human eyes [21], [22] compared to other metrics like peak signal-to-noise ratio (PSNR). Given two images  $x$  and  $y$ , SSIM can be calculated as:

$$SSIM(x, y) = \frac{(2\mu_x\mu_y + C_1)(2\sigma_{xy} + C_2)}{(\mu_x^2 + \mu_y^2 + C_1)(\sigma_x^2 + \sigma_y^2 + C_2)}, \quad (7)$$

where  $\mu_x$  is the average of  $x$ ,  $\mu_y$  is the average of  $y$ ,  $\sigma_x^2$  is the variance of  $x$ ,  $\sigma_y^2$  is the variance of  $y$ , and  $\sigma_{xy}$  is the covariance of  $x$  and  $y$ .  $C_1$  and  $C_2$  are constants for maintaining stability. Higher SSIM indicates stronger similarity between  $x$  and  $y$ . It ranges from 0 to 1 and when the two images are identical, the value equals 1.

### B. Model and Training Details

1) *Model Architecture*: We use the same model architecture for all experiments presented in this paper, a classic 2D U-Net [19], as shown in Fig. 3. The model includes an encoder and a decoder. The encoder consists of 5 blocks, each of

2) *Training Configurations*: During the training stage, we use Adam [23] as the optimizer with a learning rate of  $1e-4$ , a weight decay of  $5e-5$ , and a batch size of 20. We set 10,000 iterations for the pre-training stage and 1,000 iterations for the fine-tuning stage. Cross-entropy is used as the loss function and Dice score is chosen as the metric to evaluate the segmentation performance. The model is implemented using

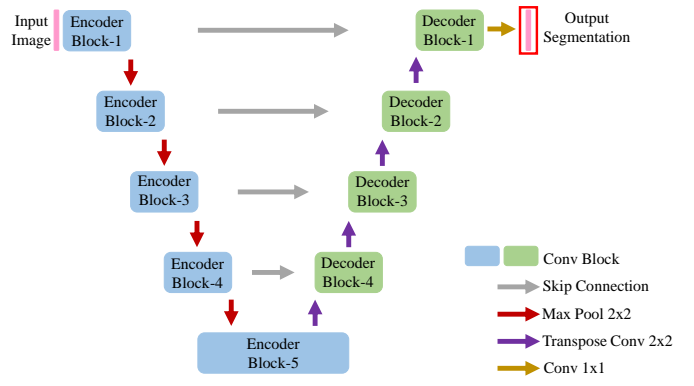


Fig. 3. U-Net architecture. Parameters of convolutional blocks in blue are frozen during the fine-tuning stage. Parameters of convolutional blocks in green are updated during the fine-tuning stage. Red box indicates the feature we use to compute the transferability scores. This figure is partially reproduced from [19].

which contains 2 sub-blocks of  $3 \times 3$  convolution, batch normalization, and ReLU activation, followed by a  $2 \times 2$  max pooling layer. In the decoder, similar blocks are used, each of which is followed by a  $2 \times 2$  transpose convolution layer. The final  $1 \times 1$  convolution layer outputs a segmentation map (logits) with 2 channels. During transfer learning, we freeze the encoder and fine-tune the decoder. The final feature map (output segmentation) produced by the decoder is used to compute the transferability score.

Python 3.6.8 and the deep learning framework PyTorch 1.8.0 [24]. All experiments are conducted on a CentOS 7.6.1810 system with one GeForce RTX 3090 GPU.

### C. Spearman's Footrule

Spearman's footrule [20] measures the absolute distance between two rankings by calculating how many steps we need to move the elements in the predicted ranking, in order to make it the same as the ground truth ranking. Formally, given two rankings  $A$  and  $B$  with the same number (denoted as  $N$ ) of elements, Spearman's footrule is calculated as:

$$Spearman(A, B) = \sum_{n=1}^N |A[n] - B[n]|, \quad (8)$$

For example, if  $A = [1, 2, 3]$  and  $B = [2, 1, 3]$ , then  $Spearman(A, B) = |1 - 2| + |2 - 1| + |3 - 3| = 2$ .